Condition assessment of underground corroded pipelines subject to hydrogen damage and combined internal pressure and axial compression

Qin, Guojin; Zhang, Zhenwei; Hou, Xiangqin; Lu, Hongfang; Huang, Y.; Wang, Yihuan

Important note
To cite this publication, please use the final published version (if applicable).
Please check the document version above.

Condition assessment of underground corroded pipelines subject to hydrogen damage and combined internal pressure and axial compression

Guojin Qin [a,b,c], Zhenwei Zhang [a,b], Xiangqin Hou [a,b], Hongfang Lu [d], Y. Huang [e], Yihuan Wang [a,b,c,*]

[a] *School of Civil Engineering and Geomatics, Southwest Petroleum University, Chengdu, Sichuan 610500, China*
[b] *Sichuan Engineering Research Center for Gas Safety and High-Efficiency Utilization, Southwest Petroleum University, Chengdu, Sichuan 610500, China*
[c] *School of Naval Architecture, Ocean and Civil Engineering, Shanghai Jiao Tong University, Shanghai, 200240, China*
[d] *China-Pakistan Belt and Road Joint Laboratory on Smart Disaster Prevention of Major Infrastructures, Southeast University, Nanjing 210096, China*
[e] *Safety and Security Science Section, Department of Values, Technology, and Innovation, Faculty of Technology, Policy, and Management, Delft University of Technology, 2628 BX Delft, The Netherlands*

ABSTRACT

In this work, a 3D finite element (FE) based model was developed to assess the condition of an underground hydrogen transmission pipeline containing a corrosion defect under combined internal pressure and soil movement-induced axial compression. The use of mechanical properties of X100 pipeline steel under different hydrogen charging time models the degree of hydrogen damage in pipelines. Parameter effects, i.e., axial compressive stress, hydrogen damage, defect geometries, and pipeline diameter-to-thickness ratio, were determined. The results demonstrated that the synergistic effect of axial compression, internal pressure, corrosion, and hydrogen damage can lead to a significant decrease in the failure pressure of pipelines. The failure pressure decreased with the wall thickness reduction and increased hydrogen damage, axial compressive stress, defect length, defect depth, and pipe diameter. The competitive effect was observed between the degree of metal loss and hydrogen damage in determining the burst capacity of pipelines. In situations where the pipeline integrity was severely compromised, the failure pressure exhibited minimal reduction despite the increasing severity of hydrogen damage. The stress distribution at the defect zone was influenced by axial compressive stress but remained unaffected by hydrogen damage under normal operating conditions (i.e., an internal pressure of 10 MPa). This work is expected to help operators understand the applicability of elder and in-service pipelines for hydrogen transmission.

1. Introduction

The widespread use of fossil fuels has resulted in many greenhouse gas emissions and the worsening of global climate change. According to relevant reports, approximately 80% of global energy consumption came from fossil fuels in 2020. Therefore, nations have announced a shift towards clean and environmentally friendly fuels, and a "global energy transition" is emerging toward net-zero emissions (Child et al., 2021). Hydrogen energy plays a vital role in the context of energy transition since it has numerous advantages (Arsad et al., 2022). For instance, hydrogen combustion does not produce carbon emissions or other pollutants. Also, hydrogen has a high energy content as a secondary energy source, with a heating value of up to 140.4 MJ/kg, 3–4

times that of other fossil fuels (Ogden, 1999). Hydrogen energy has extensive applications, such as serving as a fuel cell for electricity generation, providing power for households and industries, and powering fuel cell vehicles. It also plays a significant role in fields such as aviation and shipping (Miltner et al., 2010).

The transportation of hydrogen is a critical aspect of the hydrogen energy industry, and gaseous hydrogen transport technology is considered mature and practical (Sun et al., 2022). Steel pipelines are commonly used for gaseous hydrogen transportation due to their high transport capacity and ability to minimize energy loss, enabling efficient long-distance and large-scale hydrogen transport (Cheng and Cheng, 2023). However, the construction cost of new hydrogen pipelines is higher compared to other chemical energy carriers. To address this,
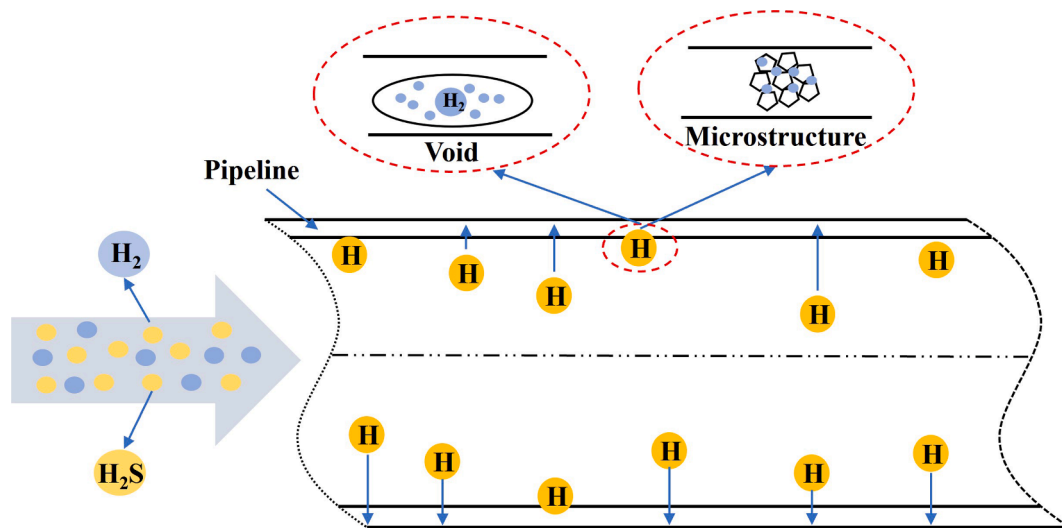
Fig. 1. Schematic diagram of the impact of hydrogen damage on pipes.

utilizing existing natural gas pipelines for hydrogen transportation or blending hydrogen into natural gas has been identified as effective cost-reduction measures (Saadi et al., 2018; Gunawan et al., 2022). These approaches take advantage of the existing infrastructure, but it is essential to consider the emerging challenges associated with hydrogen transport through steel pipelines. Hydrogen exposure increases the risk of hydrogen embrittlement (HE) in steel pipelines. Failure mode associated with HE includes hydrogen-induced cracking (HIC), hydrogen blistering (HB), and the degradation of mechanical properties in pipeline steel (Cheng, 2023; Elazzizi et al., 2015; Louthan and Caskey, 1976). Extensive research has been conducted to understand the failure mechanism of pipeline steel in hydrogen environments through tests, and modeling (Sun and Cheng, 2022). These studies have highlighted the significant impact of hydrogen damage on critical mechanical properties such as fatigue crack extension and plasticity reduction in pipeline steel (Briottet et al., 2012a, 2012b; Huang et al., 2022; Nanninga et al., 2012).

More seriously, corrosion, dents, cracks, wrinkles, and other defects will appear on the pipe with the prolongation of time. Corrosion leads to the primary mechanism of pipeline failure (Kere and Huang, 2022). According to CEPA (2019), more than 40% of incidents on oil and gas pipelines in Canada were due to corrosion between 2014 and 2018. The PHMSA (2020) report states that 20% of hazardous liquid pipeline incidents in the United States from 2010 to 2019 were caused by corrosion. EGIG (2020) reported that corrosion was the leading cause of 26.63% of pipeline incidents in Europe from 2010 to 2019. Corrosion effects results in localized thinning of the pipeline wall, which causes a burst at defect zones when the remaining wall thickness cannot withstand the internal pressure (Gong and Zhou, 2017). Predicting the burst pressure of corroded pipelines is a critical aspect of pipeline asset management (Qin and Cheng, 2021). Advanced techniques like Level-3-based finite element (FE) modeling have been developed to provide accurate predictions, incorporating factors such as defect geometries, steel grades, and interactions between multiple corrosion defects (Qin et al., 2023; Xu and Cheng, 2012). While previous studies have primarily focused on single-loading conditions, particularly internal pressure, it is essential to recognize that underground pipelines experience combined loading conditions (Ali et al., 2022; Chiodo and Ruggieri, 2009; Wang et al., 2020). Axial compressive stress can arise from various sources, including soil settlement, backfill loads, traffic loads, external construction activities, disasters, and thermal expansion restrictions (Xu and Cheng, 2012; Zhang and Zhou, 2022; Guo et al., 2023a, 2023b; Liu et al., 2023; Wang et al., 2022). Buried pipelines may face both internal pressure and axial compressive stress, resulting in reduced burst

capacity for corroded pipelines (Shuai et al., 2022; Wijewickreme et al., 2009). Excessive axial compressive stress can have detrimental effects on underground pipelines, such as deformation, buckling, or even failure, leading to significant energy and economic losses (Bruere et al., 2019; Shuai et al., 2022; Lu et al., 2023). To date, comprehensive research investigating the coupling effects of corrosion, hydrogen damage, and the combined internal pressure and axial compression on the burst capacity of pipelines remains limited. Therefore, it is crucial to gain a thorough understanding of these combined effects to properly assess the suitability of utilizing in-service natural gas pipelines for hydrogen transportation.

In this work, a FE-based model was developed to implement a condition assessment for an X100 hydrogen transmission pipeline containing a corrosion defect under combined internal pressure and axial compression. The developed model was validated through burst test data. The distributions of von Mises stress at a corrosion defect were modeled under various hydrogen charging time to demonstrate the different degrees of hydrogen damage effects. Key factors such as defect geometries, applied loadings, and pipeline geometries were modeled to determine their impact on the failure pressure of a corroded pipeline subjected to hydrogen damage. The findings of this work contribute to a better understanding of the failure behavior of hydrogen transmission pipelines to aid in optimizing pipeline design and integrity management strategies in the presence of hydrogen damage.

2. FE modeling

2.1. Hydrogen-induced degradation process of mechanical properties of pipeline steel

A phenomenon known as HE may occur on pipeline steel during the transportation of gaseous hydrogen at high pressure. It begins with the formation of hydrogen atoms through dissociative adsorption of hydrogen molecules (Capelle et al., 2013). These hydrogen atoms are then absorbed into the pipeline steel and diffuse through interstitial spaces within the material (Titov et al., 2019). As the hydrogen atoms diffuse, they tend to accumulate and concentrate in specific interstitial structures, forming what is commonly referred to as "hydrogen traps." These traps can include various metallurgical defects such as dislocations, grain boundaries, phase boundaries, inclusions, and secondary phase particles. These defects have higher hydrogen binding energy compared to the lattice fraction of the steel, making them attractive sites for hydrogen atom adsorption. As the concentration of hydrogen atoms at these traps increases, a critical threshold is eventually reached.

Table 1

Mechanical properties of the X100 steel pipeline under different hydrogen charging times.

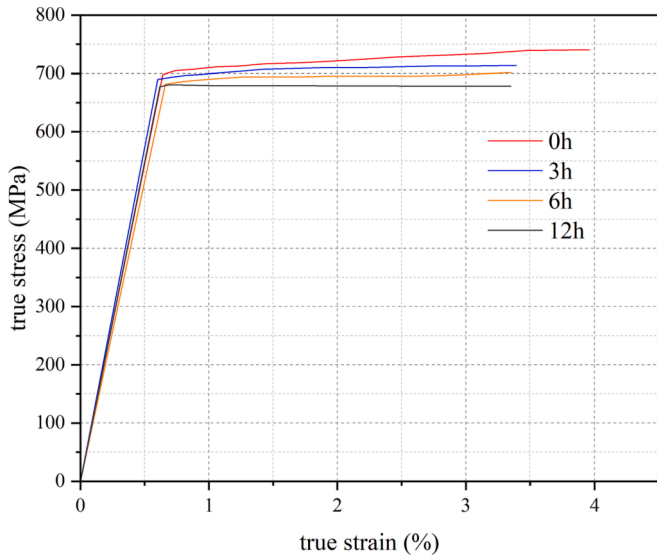| t (h)	E(GPa)	μ	σ_y(MPa)	σ_u(MPa)
0	110	0.3	698	748
3	114	0.3	690	714
6	110	0.3	681	701
12	109	0.3	677	680

Fig. 2. Stress–strain curves of X100 pipeline steel under different hydrogen charging times.

According to theories such as hydrogen enhanced localized plasticity (HELP), hydrogen enhanced decohesion (HEDE), or their synergistic effect, when the hydrogen content is sufficiently high, cracks can be initiated under stress or even in the absence of stress (Djukic et al., 2019), which poses a severe risk to pipeline integrity. The aggregation of hydrogen atoms at the hydrogen traps forms aggregates that can grow and join with other defect sites in the steel, such as corrosion defects and cracks. These aggregated defects can cause a degradation of the steel's mechanical properties, such as elongation, fracture toughness, yield strength and tensile strength. In high-pressure environments, the presence of these defects can ultimately lead to steel fracture (Barrera et al., 2018). Fig. 1 shows a schematic diagram of the impact of hydrogen damage on pipes (Zhang and Tian, 2022).

2.2. Material and failure criterion of the pipeline subjected to hydrogen damage

The severity of hydrogen-induced degradation depends on several factors, such as the exposure time (Kittel et al., 2010). Thus, the general idea in this work of modeling hydrogen damage is using the mechanical properties of the pipeline steel under various hydrogen charging time. The real stress–strain data of X100 pipeline steel under different hydrogen charging time were obtained by the uniaxial tensile tests of Wang et al. (2018). Table 1 shows the mechanical properties of the pipeline under hydrogen charging time of 0 h (i.e., modeling pipeline in the air), 3 h, 6 h, and 12 h, respectively, including Young's modulus (E), Poisson's ratio (μ), yield strength (σ_y), and ultimate tensile strength (σ_u). Fig. 2 shows the stress–strain curves of X100 pipeline steel under different hydrogen charging time. It is worth noting that this method is suitable for modeling hydrogen damage of pipeline steel in pure hydrogen or a mixture of hydrogen and natural gas.

Internal pressure is the primary source of stress on the pipeline, and the failure criterion used in this work is based on the ultimate strength theory (UST), that is, the pipeline fails if the von Mises stress of any point at the corrosion defect reaches the ultimate tensile strength of the pipeline steel. The corresponding internal pressure applied is defined as the failure pressure of the pipeline. The criterion has also been proven to be accurate in some previous works (Xu and Cheng, 2012; Chen et al., 2015; Qin et al., 2023).

2.3. Initial and boundary conditions

All FE modeling was implemented using ABAQUS® 2022. Fig. 3 shows the developed 3D FE-based model of the X100 pipeline containing an external corrosion defect. Due to the symmetry of the model geometries and loadings, a quarter FE model was developed to save calculation costs. For reasonable and convenient defect assessment, idealized methods were adopted to simplify the corrosion defect due to the actual defect shape being too complex (Zhang and Tian, 2022). The defect zone was modeled as a rectangle based on the well-known B31G modified method (Qin and Cheng, 2021; Sun and Cheng, 2018). The edges of the corrosion defect were modeled as smooth to prevent a stress concentration (Huang et al., 2022). Table 2 lists the defect geometries. The pipeline length is long enough to avoid the influence of boundary conditions on the corroded area.

Fig. 4 shows the boundary conditions setting of the developed FE model. Y-axis symmetric constraints were applied to the bottom and top symmetrical surfaces of the pipeline. The use of Z-axis symmetric constraints was placed on the near-end surface. To maintain the stability of the pipeline under combined loadings, a fully fixed constraint was applied at a point at the bottom of the right end. The defect-free end was completely free. For combined loadings, the internal pressure was applied to the inner wall of the pipeline, while the axial compression (σ_a) was introduced by applying a uniform compressive stress on a
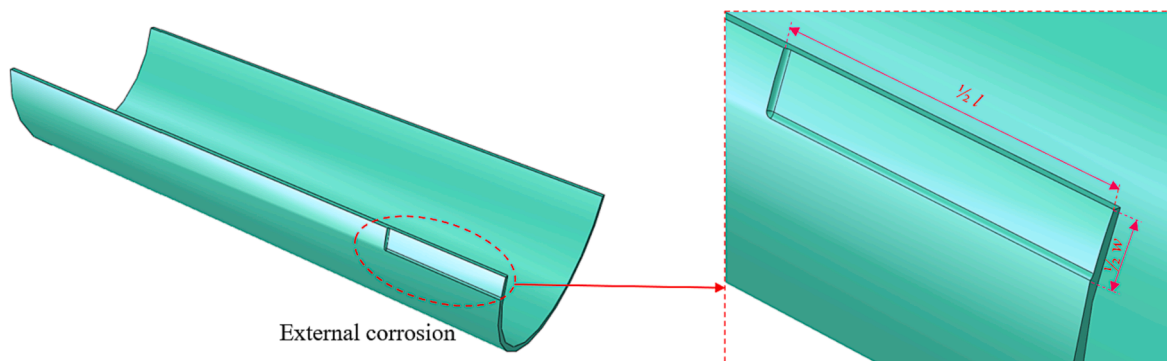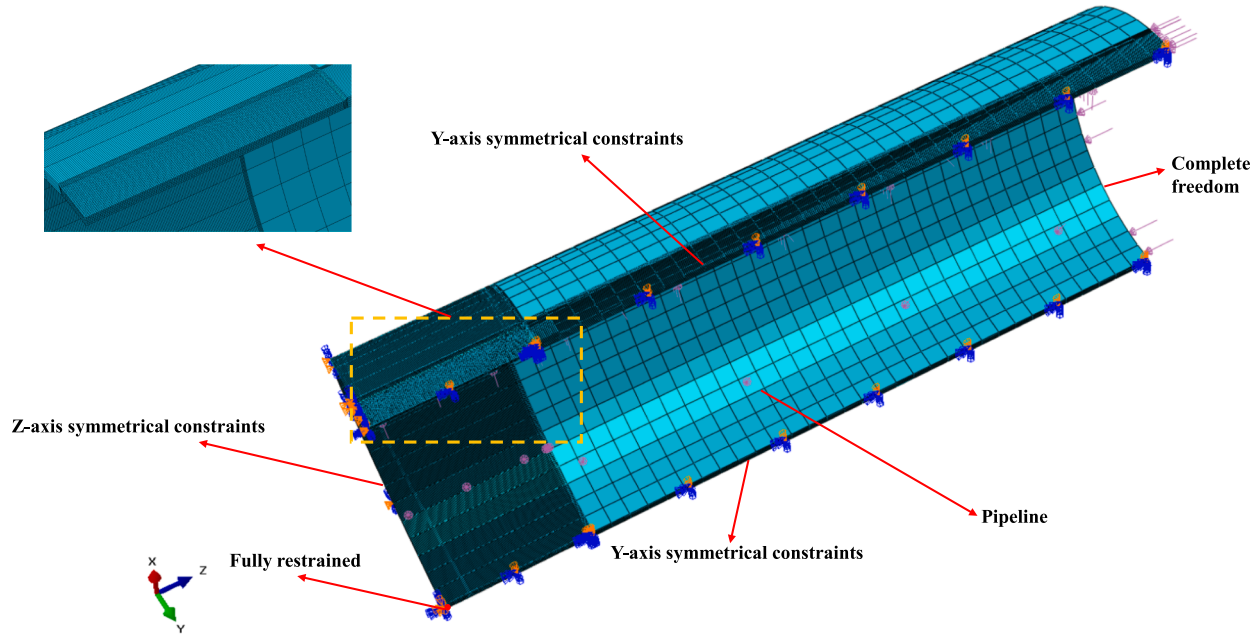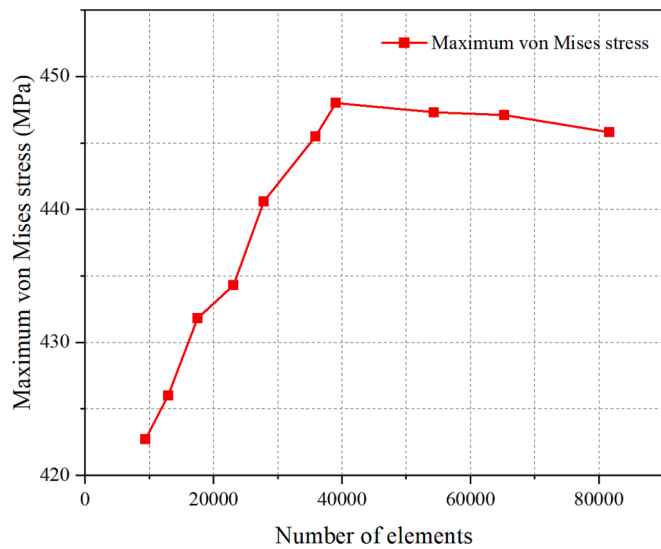

Fig. 3. FE model of the corrosion defect.

Table 2
Base conditions for parametric FE modeling.

Variable	Axial compression stress	Internal pressure	Pipeline				Steel grade	Defect		
			D	t	D/t			L	W	δ
Value	$0.2\sigma_y$	10 MPa	818.2 mm	19.1 mm	42.8		X100	800 mm	30°	0.6 t

Fig. 4. Meshing details and boundary conditions of the FE model.

Fig. 5. Mesh sensitivity analysis.

corrosion-free cross-section at the free end of the FE model (Zhang and Zhou, 2022). Mesh quality is critical to the modeling results. Eight-node linear hexahedral elements (i.e., C3D8R) were used for meshing the FE model. The refined meshes were used at the defect zone, while the remainder was coarsened. Mesh sensitivity analysis was performed to determine a suitable mesh size and amount. As shown in Fig. 5, the maximum von Mises stress at the corrosion defect tends to be stable when the number of elements exceeds 39050. After reaching 54324, the

modeling result is no longer affected by the mesh number. The mesh size of the defect area is 2.5 mm, while that of the pipe body is 50 mm.

2.4. Analysis procedure

Failure behavior was modeled at a single corrosion defect on a X100 steel-made pipeline subjected to combined loading of internal pressure and axial compressive stress as well as different hydrogen damage. Control variable analysis method-based parameter studies included the modeling of hydrogen damage, axial compressive stress, defect length, and depth, as well as the diameter-to-thickness ratio. The magnitude of axial compressive stress (σ_a) was modeled using ratios to σ_y, i.e., σ_a/σ_y=-0.05, −0.10, −0.15, −0.20, and −0.25. To consider the defect growth, the defect geometries (i.e., defect depth and length) were modeled in various. The defect length was modeled as 200, 400, 600, 800, and 1000 mm. The use of defect depth-to-wall thickness ratio modeled various defect depths, i.e., 0.2, 0.3, 0.4, 0.5, and 0.6. The diameter-to-thickness ratio of the pipeline was set as 40, 42.8, 45.6, 48.4, and 51.2 to model the various pipeline geometries. The pipe

Table 3
Failure pressure of corroded pipelines from tests and FE modeling.

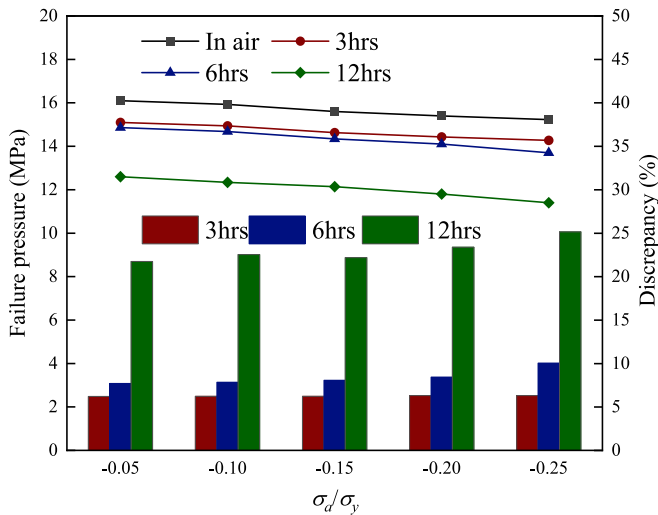| NO.	Pipe diameter D (mm)	Wall thickness t (mm)	Defect depth δ (mm)	Defect length l (mm)	Results		
					P_{test} (MPa)	P_{FEM} (MPa)	RE (%)
1	408.2	6.2	0.33t	346	14.60	14.31	1.97
2	407.4	5.9	0.57t	142	12.72	12.18	4.25
3	407.4	6.0	0.87t	346	12.84	12.34	3.89
4	610.5	6.8	0.3t	742	14.21	13.76	3.17
5	610.5	3.7	0.39t	412	14.37	14.04	2.30

Fig. 6. Failure pressure and discrepancy of X100 corroded pipes under different axial compression stress and hydrogen damage.

diameter was fixed at 818.2 mm, while the wall thickness wass 20.4, 19.1, 17.9, 16.9, and 16 mm, respectively. The wall thickness was 19.1 mm, and the pipe diameter will be 764, 818.2, 871, 924, and 977 mm. Table 2 lists the base conditions for the FE modeling. Note when one variable changes, others are fixed.

3. Result and discussion

3.1. Verification of FE model

Table 3 shows five burst test data obtained from the work of Bhardwaj et al. (2021) to validate the developed FE model. The relative error (RE) was determined by comparing the results obtained from the FE modeling with the corresponding burst test data, using Eq. (1). The analysis reveals that the REs between the test results and the modeling outcomes are all below 4.5%. The lowest RE recorded is 1.97%, while the highest RE observed is 4.25%. These results demonstrate the feasibility and accuracy of the developed FE model in predicting failure pressure. Furthermore, they validate the appropriateness and soundness of the meshing, initial and boundary conditions, and failure criteria

employed in the model.

$$Relative\ error = \left(|P_{test} - P_{FEM}|\right)/P_{test} \times 100\% \qquad (1)$$

where P_{test} is the data of burst test; P_{FEM} is the failure pressure obtained by FE modeling.

3.2. Effect of axial compressive stresses on the failure pressure of a hydrogen transmission pipeline containing a corrosion defect

Fig. 6 illustrates the relationship between failure pressure and discrepancy in X100 corroded pipelines under various compressive stresses. Generally, the failure pressure of the pipeline decreases as the axial compressive stress increases. For instance, as σ_a/σ_y increases from 0.05 to 0.25, the failure pressure of the pipeline in the air decreases by 0.9 MPa. This decrease in failure pressure can be attributed to the increased stress concentration at the defect zone caused by the additional stress (Mondal and Dhar, 2019). A column diagram is presented to quantify the discrepancy in failure pressure between corroded pipelines transporting hydrogen and natural gas, with the latter serving as the benchmark. A higher column indicates a more significant discrepancy. Evidently, the failure pressure of corroded pipelines decreases with a longer hydrogen charging time. The discrepancy remains around 6% and 8% when the hydrogen charging time is 3 and 6 h, respectively, and this discrepancy does not change with increasing loading. However, the discrepancy becomes significant when the hydrogen charging time reaches 12 h. For instance, when σ_a/σ_y is −0.25, the discrepancy is close to 25%, indicating a substantial decrease in the local residual strength of the pipeline due to high hydrogen damage. Under identical loading conditions, increasing the hydrogen charging time leads to a reduction in the failure pressure of corroded pipelines. For instance, when the σ_a/σ_y is −0.05, the failure pressure of a corroded pipeline in the air is 16.1 MPa. With a hydrogen charging time of 3 h, the failure pressure decreases by 6%. Further reductions in failure pressure occur as the magnitude of hydrogen damage increases, e.g., at 6 and 12 h of hydrogen charging time.

Fig. 7 presents the distributions of von Mises stress at the defect zone on a X100 hydrogen pipeline under internal pressure of 10 MPa and different axial compressive stresses. It is found that a stress concentration zone is observed at the edge of the defect. While a lower stress zone is observed at the corrosion center. With increased axial compressive stress, the high-stress region gradually expands towards the defect
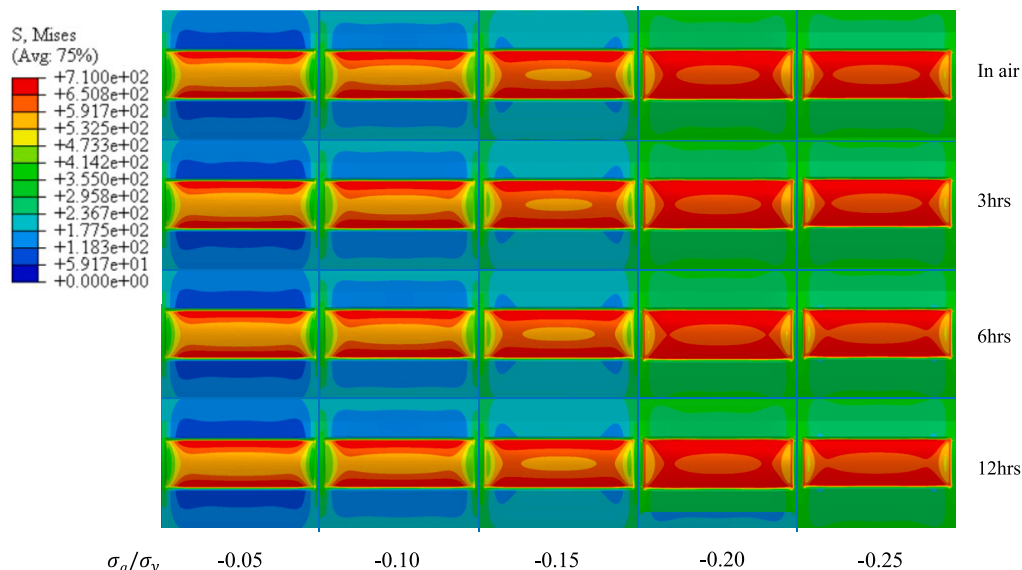

Fig. 7. The distributions of von Mises stress at the defect zone on a pipeline subjected to hydrogen damage under different axial compressive stresses.
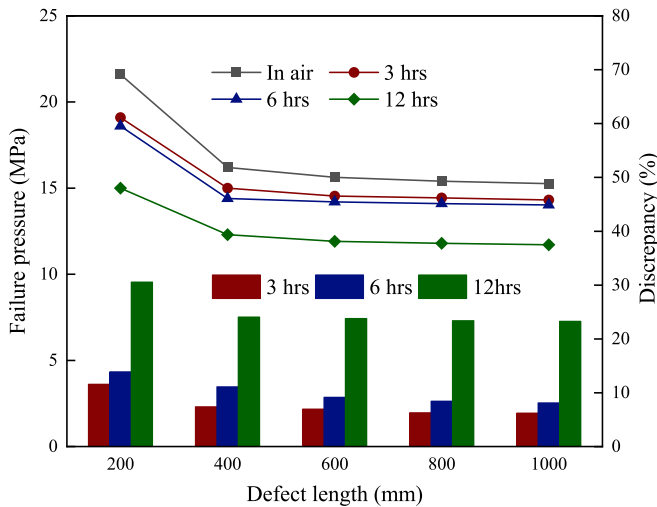
Fig. 8. Failure pressure and discrepancy of a X100 corroded pipeline subjected to hydrogen damage under different defect lengths.

center. However, it is worth noting that the increase in hydrogen charging time (i.e., hydrogen damage increases) does not significantly affect the stress distribution, indicating that hydrogen damage has little impact on the mechanical stress field under normal operating conditions (i.e., an internal pressure of 10 MPa).

3.3. Effect of defect geometries on the failure pressure of hydrogen pipelines containing a corrosion defect

(1) Defect length

Fig. 8 shows the failure pressures and discrepancy of X100 hydrogen pipelines containing a corrosion defect with different defect lengths. With the same hydrogen damage, the failure pressure of the pipeline exhibits a notable decrease as the defect length increases from 200 mm to 400 mm. Additionally, it can be observed that as the hydrogen charging time (Hydrogen damage) increases, the reduction in pipeline failure pressure diminishes gradually with the corresponding rise in

defect length. For instance, the failure pressure decreases by 22.18% when subjected to a hydrogen charging time of 3 h. However, the decrease in failure pressure is observed to be 15.23% with an extended hydrogen charging time of 12 h. After the defect length exceeds 400 mm, the failure pressure of the pipeline no longer exhibits a significant decrease as the defect length continues to increase. Under base conditions, the failure pressure of a pipeline with a corrosion defect of the same length exhibits a significant decrease as the hydrogen damage increases. However, as the defect length increases, the discrepancy in failure pressure gradually diminishes. For example, when the defect length is 200 mm and the hydrogen charging time is 12 h, the discrepancy exceeds 30%; that decreases to below 25% when the defect length reaches 600 mm. The most plausible explanation is that hydrogen damage and the degree of metal loss compete to determine the burst capacity of corroded pipelines.

Fig. 9 illustrates the distributions of von Mises stress at the corrosion defects with different lengths on a hydrogen pipeline. Near the corrosion edges, high-stress zones are more likely to appear. As the defect length increases, these high-stress areas exhibit a wider distribution, and this trend becomes more stable. Furthermore, while the hydrogen charging time increases the degree of hydrogen damage, its impact on the stress distribution at the same defect length is slight and can even be negligible.

(2) Defect depth

Fig. 10 shows the failure pressure and discrepancy of the X100 hydrogen pipeline containing a corrosion defect with different depths. Generally, the failure pressure of the pipeline significantly decreases with increasing defect depth under the same degree of hydrogen damage. In particular, when the hydrogen charging time is 12 h, the failure pressure drops by 50.64% from a δ/t of 0.2 to 0.6, demonstrating a significant influence. This is because the structural integrity of the pipeline is compromised. The defect acts as a stress concentration point, where the stress distribution becomes uneven and localized, leading to a reduction in the overall strength of the structure. An interesting observation is that when the δ/t reaches 0.6, the failure pressure of the corroded pipeline with hydrogen charging time of 3 h and 6 h is similar, both around 14.2 MPa. This suggests that hydrogen damage has little impact on the failure pressure of the pipeline when the local wall
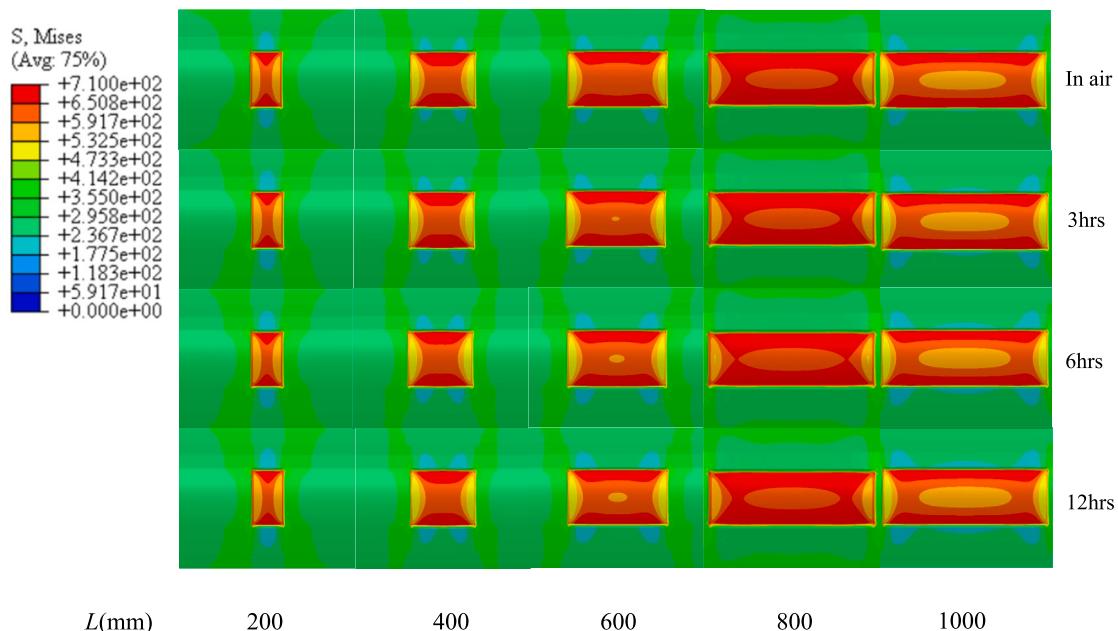

Fig. 9. The distributions of von Mises stress at the defect zone on a pipeline with different defect lengths and hydrogen charging times.
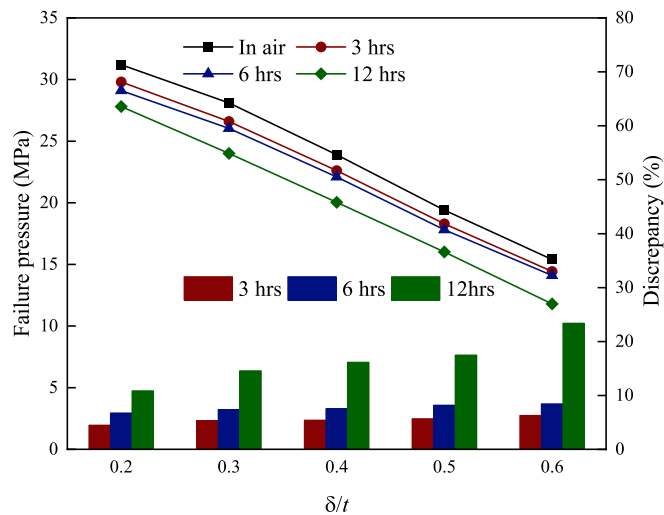
Fig. 10. Failure pressure and discrepancy of a X100 pipeline containing a corrosion defect with different depth and hydrogen charging times.

thickness is relatively thin. When considering the effect of hydrogen damage, the decrease in failure pressure is not as pronounced. Generally, the discrepancy increases with the increase of defect depth. While hydrogen damage can lead to material degradation and embrittlement, the reduction in failure pressure attributed solely to hydrogen damage is relatively minor compared to the decrease caused by an increase in defect depth. For example, the failure pressure of the pipeline in the air decreases by about 23% when the hydrogen charging time increases to 12 h.

Fig. 11 shows the distribution of von Mises stresses at a corrosion defect with different depths on a pipeline subjected to hydrogen damage. When the δ/t is relatively small, less than 0.4, the stress distribution within the corroded area appears uniform. This indicates that the pipeline is experiencing elastic deformation, and the stresses are evenly distributed across the corrosion defect. As the defect depth increases, the distribution of von Mises stress becomes more sensitive to changes. Once the δ/t reaches 0.5, stress concentration and plastic deformation occur

predominantly at the edge of the corrosion zone. This signifies a transition to the plastic deformation stage, where higher stresses become localized near the defect edges. The high-stress region becomes even more concentrated when the defect depth grows, exacerbating the corrosion damage. This implies that deeper defects result in more pronounced stress concentration and increased plastic deformation, which heightens the risk of failure. It is worth noting that under base conditions, with the presence of hydrogen damage, the stress distribution at a corrosion defect with the same defect depth remains unaffected. This suggests that hydrogen damage, in this specific context, does not substantially impact the stress distribution characteristics.

3.4. Effect of diameter-to-thickness ratio on the failure pressure of hydrogen pipelines with a corrosion defect

(1) Wall thickness of the pipeline

Fig. 12 shows the failure pressure and discrepancy of a corroded X100 pipeline presented as a function of diameter-thickness ratios (D/t) with various wall thicknesses of the pipeline. This analysis considers variations in wall thickness (Outer diameter is fixed) and the presence of hydrogen damage. It is evident that the failure pressure of the corroded pipeline decreases as the D/t increases. This decrease is observed irrespective of the presence of hydrogen damage. This can be attributed to the fact that as the wall thickness decreases, the local strength of the pipeline diminishes. As D/t increases, which corresponds to a decrease in the wall thickness of the pipeline, the discrepancy between different hydrogen charging time becomes little. For example, with a D/t of 40, the maximum discrepancy is 16.1% between different hydrogen charging time, whereas the maximum discrepancy decreases to 8.8% with a D/t of 51.2. It is demonstrated that the influence of hydrogen damage on the failure pressure becomes less pronounced as the wall thickness decreases. It may be explained that the stress concentration caused by the reduced material thickness becomes dominant compared to the influence of hydrogen damage when the wall thickness is already thin.

Fig. 13 shows the distributions of von Mises stress at a corrosion defect on a pipeline with variations in the pipe wall thickness and hydrogen damage. It can be observed that under the same hydrogen
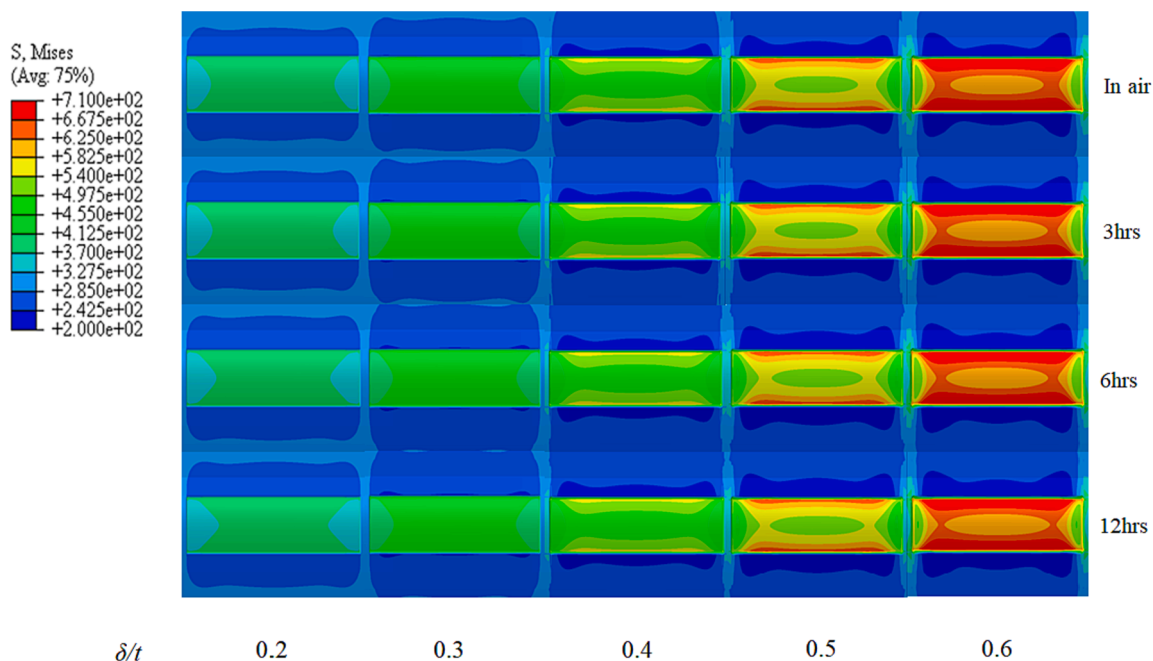

Fig. 11. The distribution of von Mises stress at the defect region with different defect depths and hydrogen charging times.
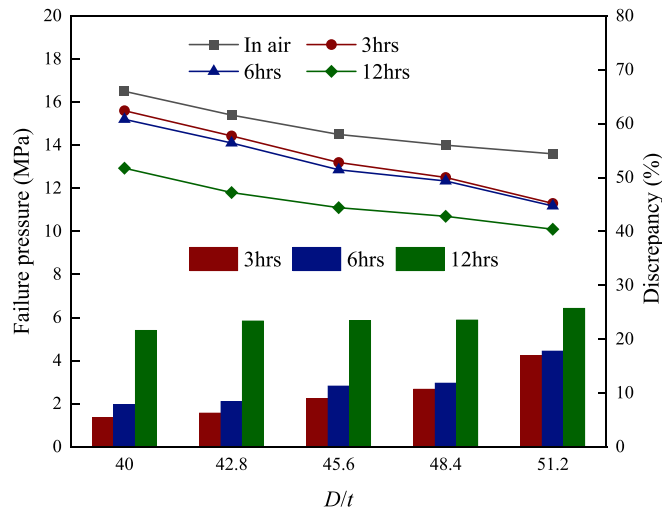
Fig. 12. Failure pressure and discrepancy of X100 corroded pipeline hydrogen damage as a function of different diameter-thickness ratio under variations of wall thickness.

X100 pipeline subjected to hydrogen damage as a function of diameter-thickness ratios (D/t) with varying outer diameters. In general, the failure pressure of the corroded pipeline decreases as the pipe diameter increases. However, interestingly, the failure pressure has little change with increasing pipe diameter when the hydrogen charging time is 12 h. In other words, the outer diameter has little impact on the failure pressure of corroded pipelines subjected to high hydrogen damage. When examining the discrepancy in failure pressures between different levels of hydrogen damage and the conventional operating environment (air) for the corroded pipeline, it is observed that at lower levels of hydrogen damage (with hydrogen charging time of 3 h and 6 h), the discrepancy remains consistent irrespective of the pipe diameter. Nevertheless, for a hydrogen charging time of 12 h, the discrepancy decreases as the outer diameter grows. This means that the impact of hydrogen damage on the failure pressure becomes less significant with larger pipe diameters when the hydrogen charging time is extended.

Fig. 15 illustrates the distributions of von Mises stress at a corrosion defect on a pipeline considering variations in the outer diameter and hydrogen damage under a combined internal pressure of 10 MPa and

charging time, the decrease in wall thickness leads to a more pronounced stress concentration, resulting in localized high-stress areas at the defect zone. For example, when the hydrogen charging time is 12 h, and the diameter-to-thickness ratio is 42.8, the low-stress area at the defect center is observed as an elliptical. Still, when the diameter-to-thickness ratio is 51.2, the low-stress area disappears, and a high-stress level occurs defect root. It is interesting to find that, except for the case of a diameter-to-thickness ratio of 51.2, an increase in hydrogen damage leads to the expansion of the low-stress area at the defect center on the pipeline with the same diameter-to-thickness ratio as shown in light red. This can be attributed to the effects of hydrogen-induced degradation on the mechanical properties and behavior of the pipeline steel. Hydrogen damage can reduce the ductility and strength of the pipeline material, leading to a redistribution of stresses.

(2) Outer diameter of the pipeline

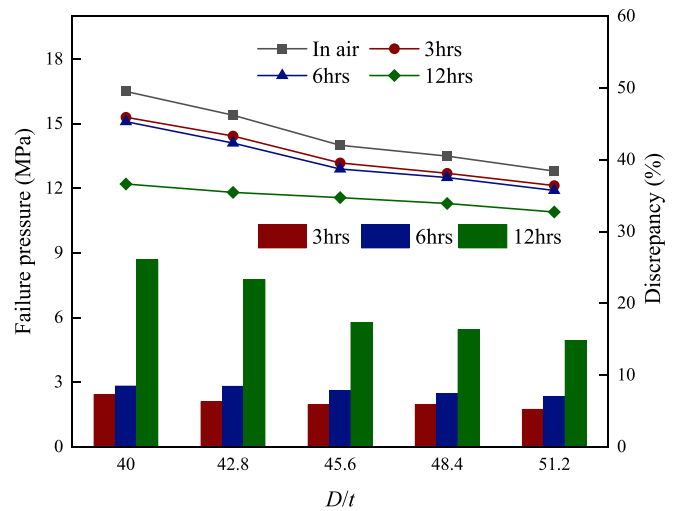Fig. 14 illustrates the failure pressure and discrepancy of a corroded

Fig. 14. Failure pressure and discrepancy of X100 corroded pipeline subjected to hydrogen damage under different outer diameter of pipelines.
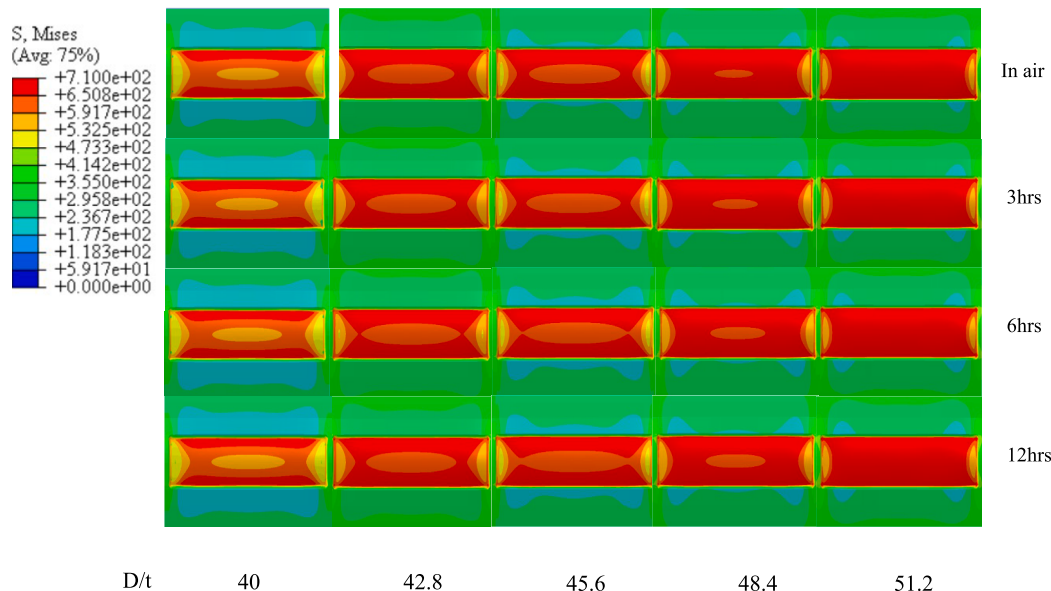

Fig. 13. The distributions of von Mises stress at a corrosion defect on a pipeline with variations of wall thickness and hydrogen damage.
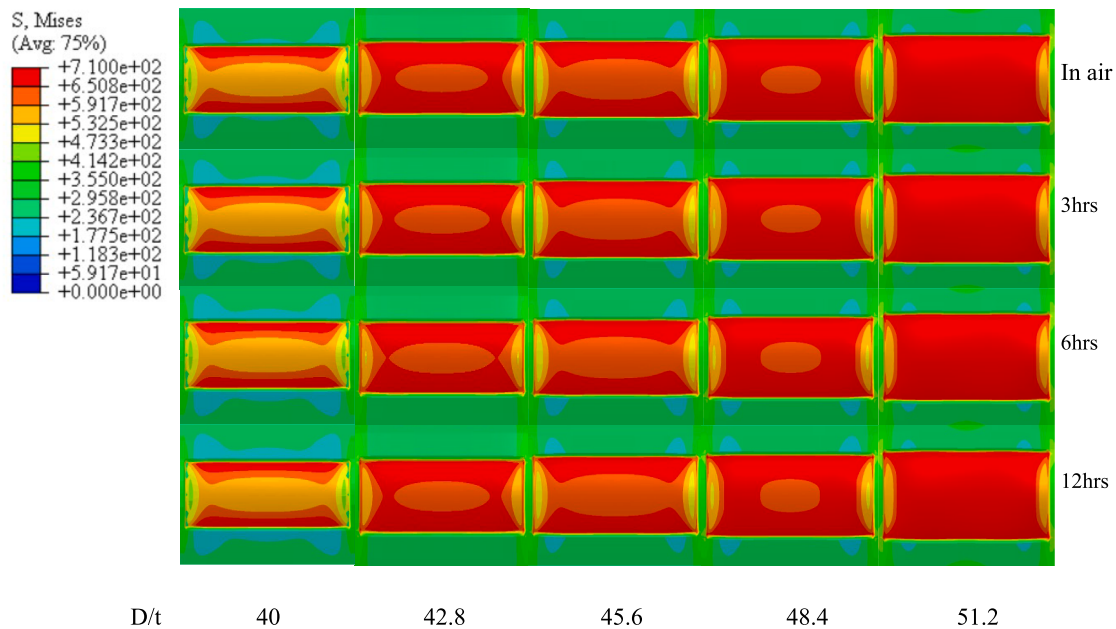
Fig. 15. The distributions of von Mises stress at a corrosion defect on a pipeline with variations of the pipe diameter and hydrogen damage.

axial compressive stress. It can be found that the stress level at the defect zone generally rises as the diameter-to-thickness ratio increases, indicating that higher diameter-to-thickness ratios lead to higher stress concentrations on the corroded pipeline. With a hydrogen charging time of 12 h and a diameter-to-thickness ratio of 40, a high-stress area is observed at the edge of the defect. This indicates that the stress concentration is prominent at the defect boundary. When the diameter-to-thickness ratio is further increased to 51.2, the stress distribution becomes more uniform throughout the defect area. In this case, the stress level increases, demonstrating a more severe stress concentration throughout the defect region. It is worth noting that the increase in hydrogen damage has little impact on the low-stress zone at the center of the defect for pipes with the same diameter-to-thickness ratio, as shown in light red and light yellow.

3.5. Discussion

The mechanical properties of X100 pipeline steel utilized for FE modeling were determined through electrochemical hydrogen charging tests conducted by Wang (2018). However, these test results may not fully represent the real-world conditions experienced in hydrogen-doped natural gas pipelines. In actual hydrogen-doped natural gas pipelines, a significant amount of gaseous hydrogen enters the interior of the pipeline steel in the form of hydrogen atoms, following dissociation and adsorption processes. This occurrence triggers the HE phenomenon, resulting in the degradation of the mechanical properties of the pipeline steel (Jia et al., 2023). It is crucial to recognize that the degradation of mechanical properties caused by gaseous hydrogen differs substantially from the effects of electrochemical hydrogen charging (Cai et al., 2022). As such, it is imperative to conduct further evaluations to understand the impact of gaseous hydrogen on pipeline integrity after it enters the pipeline steel in the form of hydrogen atoms. By doing so, we can enhance the applicability and relevance of our research and ensure a more accurate representation of the challenges faced in hydrogen-doped natural gas pipelines.

4. Conclusions

In this work, a validated FE model was developed to predict the failure pressure of a hydrogen pipeline containing a corrosion defect under combined internal pressure and axial compressive stress. The main factors influencing the failure pressure of hydrogen pipelines, including the degree of hydrogen damage, combined loadings, defect geometries, and pipeline geometries, were identified. The failure pressure of the pipeline decreases with increasing axial compressive stress, mainly due to stress concentration at the defect zone. Longer hydrogen charging time decrease failure pressure, indicating the detrimental effect of hydrogen damage. The discrepancy in failure pressure between corroded pipelines transporting hydrogen and natural gas is significant at a higher hydrogen charging time, emphasizing the impact of hydrogen damage on the local residual strength of the pipeline. The stress distribution at the defect zone is influenced by axial compressive stress but remains unaffected by hydrogen damage under normal operating conditions (i.e., an internal pressure of 10 MPa). Defect length affects the failure pressure, with longer defects leading to more pronounced reductions. However, the discrepancy in failure pressure diminishes as hydrogen charging time increases. Defect depth also influences the failure pressure, with deeper defects causing a significant decrease. Hydrogen damage has a relatively minor impact on the failure pressure compared to the effect of defect depth. The diameter-thickness ratio of the pipeline affects the failure pressure, with a decrease in wall thickness leading to decreased failure pressure. The outer diameter has little impact on the failure pressure for pipelines subjected to high hydrogen damage. On the other hand, this study investigates the mechanical response of hydrogen-damaged steel pipelines by modeling the von Mises stress distribution at corrosion defects under different hydrogen charging time. This can more accurately identify high-stress areas and provide guidance for designing reliable pipeline structures. At the same time, it provides a deeper understanding of the failure behavior of transmission pipelines under hydrogen damage conditions. This can help operators promptly identify possible pipeline weaknesses, explore the critical failure mechanisms caused by hydrogen damage, and propose corresponding pipeline optimization design solutions and integrity management strategies. Overall, the findings of this work provide insights into the integrity of aged pipelines subjected to hydrogen damage, emphasizing the importance of considering various factors in pipeline design and maintenance practices.

CRediT authorship contribution statement

Guojin Qin: Conceptualization, Methodology, Writing – review & editing, Formal analysis, Project administration, Funding acquisition. **Zhenwei Zhang:** Investigation, Software, Validation, Data curation, Writing – original draft, Writing – review & editing. **Xiangqin Hou:** Writing – review & editing. **Hongfang Lu:** Writing – review & editing, Funding acquisition. **Y. Huang:** Writing – review & editing. **Yihuan Wang:** Supervision, Funding acquisition, Project administration, Writing – review & editing.

Declaration of Competing Interest

The authors declare that they have no known competing financial interests or personal relationships that could have appeared to influence the work reported in this paper.

Data availability

Data will be made available on request.

Acknowledgment

References

Ali, K., Qin, J., Faber, M.H., 2022. On information modeling in structural integrity management. Struct. Health Monit. 21, 59–71.

Arsad, A.Z., Hannan, M.A., Al-Shetwi, A.Q., Mansur, M., Muttaqi, K.M., Dong, Z.Y., Blaabjerg, F., 2022. Hydrogen energy storage integrated hybrid renewable energy systems: a review analysis for future research directions. Int. J. Hydrogen Energ. 47 (39), 17285–17312.

Barrera, O., Bombac, D., Chen, Y., Daff, T.D., Galindo-Nava, E., Gong, P., et al., 2018. Correction to: understanding and mitigating hydrogen embrittlement of steels: a review of experimental, modelling and design progress from atomistic to continuum. J. Mater. Sci. 53, 10593–10594.

Bhardwaj, U., Teixeira, A.P., Guedes Soares, C., 2021. Burst strength assessment of X100 to X120 ultra-high strength corroded pipes. Ocean Eng. 241.

Briottet, L., Batisse, R., de Dinechin, G., Langlois, P., Thiers, L., 2012a. Recommendations on X80 steel for the design of hydrogen gas transmission pipelines. Int. J. Hydrogen Energ. 37 (11), 9423–9430.

Briottet, L., Moro, I., Lemoine, P., 2012b. Quantifying the hydrogen embrittlement of pipeline steels for safety considerations. Int. J. Hydrogen Energ. 37 (22), 17616–17623.

Bruere, V.M., Bouchonneau, N., Motta, R.S., Afonso, S.M.B., Willmersdorf, R.B., Lyra, P. R.M., Torres, J.V.S., de Andrade, E.Q., Cunha, D.J.S., 2019. Failure pressure prediction of corroded pipes under combined internal pressure and axial compressive force. J. Braz. Soc. Mech. Sci. Eng. 41 (4), 1–10.

Cai, L., Bai, G., Gao, X., Li, Y., Hou, Y., 2022. Experimental investigation on the hydrogen embrittlement characteristics and mechanism of natural gas-hydrogen transportation pipeline steels. Mater. Res. Exp. 9 (4).

Canadian Energy Pipeline Association (CEPA), 2019. Pipeline Performance Report. Canada, Calgary, Alberta.

Capelle, J., Dmytrakh, I., Azari, Z., Pluvinage, G., 2013. Evaluation of electrochemical hydrogen absorption in welded pipe with steel API X52. Int. J. Hydrogen Energ. 38 (33), 14356–14363.

Chen, Y.F., Zhang, H., Zhang, J., Liu, X.B., Li, X., Zhou, J., 2015. Failure assessment of X80 pipeline with interacting corrosion defects. Eng. Fail. Anal. 47, 67–76.

Cheng, Y.F., 2023. Essence and gap analysis for hydrogen embrittlement of pipelines in high-pressure hydrogen environments. Oil & Gas Storage and Transportation. 42 (1), 1–8.

Cheng, W., Cheng, Y.F., 2023. A techno-economic study of the strategy for hydrogen transport by pipelines in Canada. J. Pipeline Sci. Eng. 100112.

Child, M., Koskinen, O., Linnanen, L., Breyer, C., 2021. Corrigendum to Sustainability guardrails for energy scenarios of the global energy transition [Renew. Sustain. Rev. (2018) 91 321-334]. Renew. Sust. Energ. Rev. 138.

Chiodo, M.S.G., Ruggieri, C., 2009. Failure assessments of corroded pipelines with axial defects using stress-based criteria: numerical studies and verification analyses. Int. J. Pres. Ves. Pip. 86, 164–176.

Djukic, M.B., Bakic, G.M., Zeravcic, V.S., Sedmak, A., Rajicic, B., 2019. The synergistic action and interplay of hydrogen embrittlement mechanisms in steels and iron: Localized plasticity and decohesion. Eng. Fract. Mech. 216, 106528.

Elazzizi, A., Hadj Meliani, M., Khelil, A., Pluvinage, G., Matvienko, Y.G., 2015. The master failure curve of pipe steels and crack paths in connection with hydrogen embrittlement. Int. J. Hydrogen Energ. 40 (5), 2295–2302.

European Gas pipeline Incident data Group (EGIG), 2020. 11th EGIG report: Period 2010–2019, Doc. Number VA 20.0432.

Gong, C., Zhou, W., 2017. First-order reliability method-based system reliability analyses of corroding pipelines considering multiple defects and failure modes. Struct. Infrastruct. E. 13 (11), 1451–1461.

Gunawan, T.A., Cavana, M., Leone, P., Monaghan, R.F.D., 2022. Solar hydrogen for high capacity, dispatchable, long-distance energy transmission – a case study for injection in the Greenstream natural gas pipeline. Energ. Convers. Manage. 273, 116398.

Guo, X., Liu, X., Li, M., Lu, Y., 2023a. Lateral force on buried pipelines caused by seabed slides using a CFD method with a shear interface weakening model. Ocean Eng. 280, 114663.

Guo, X., Fan, N., Liu, Y., Liu, X., Wang, Z., Xie, X., Jia, Y., 2023b. Deep seabed mining: frontiers in engineering geology and environment. Int. J. Coal Sci. Techn. 10 (1), 23.

Huang, Y., Qin, G., Hu, G., 2022. Failure pressure prediction by defect assessment and finite element modeling on pipelines containing a dent-corrosion defect. Ocean Eng. 266, 112875.

Jia, G., Lei, M., Li, M., Xu, W., Li, R., Lu, Y., Cai, M., 2023. Hydrogen embrittlement in hydrogen-blended natural gas transportation systems: a review. Int. J. Hydrog. Energy.

Kere, K.J., Huang, Q., 2022. Development of probabilistic failure pressure models for pipelines with single corrosion defect. Int. J. Pressure Vessels Pip. 197.

Kittel, J., Smanio, V., Fregonese, M., Garnier, L., Lefebvre, X., 2010. Hydrogen induced cracking (HIC) testing of low alloy steel in sour environment: impact of time of exposure on the extent of damage. Corrosion Sci. 52 (4), 1386–1392.

Liu, X., Wang, Y., Zhang, H., Guo, X., 2023. Susceptibility of typical marine geological disasters: an overview. Geoenviron. Disast. 10, 10.

Louthan Jr, M.R., Caskey Jr, G.R., 1976. Hydrogen transport and embrittlement in structural metals. Int. J. Hydrogen Energ. 1 (3), 291–305.

Lu, H., Xu, Z.D., Cheng, Y.F., Peng, H., Xi, D., Jiang, X., Shan, Y., 2023. an inventory of greenhouse gas emissions due to natural gas pipeline incidents in the United States and Canada from 1980s to 2021. Sci. Data 10 (1), 282.

Miltner, A., Wukovits, W., Pröll, T., Friedl, A., 2010. Renewable hydrogen production: a technical evaluation based on process simulation. J. Clean. Prod. 18, S51–S62.

Mondal, B.C., Dhar, A.S., 2019. Burst pressure of corroded pipelines considering combined axial forces and bending moments. Eng. Struct. 186, 43–51.

Nanninga, N.E., Levy, Y.S., Drexler, E.S., Condon, R.T., Stevenson, A.E., Slifka, A.J., 2012. Comparison of hydrogen embrittlement in three pipeline steels in high pressure gaseous hydrogen environments. Corros. Sci. 59, 1–9.

Ogden, J.M., 1999. Prospects for building a hydrogen energy infrastructure. Ann. Rev. Environ. Resour. 24 (1), 227–279.

Pipeline and Hazardous Materials Safety Administration (PHMSA), 2020. Pipeline Incident 20 Year Trends. Department of Transportation, Washington DC, US.

Qin, G., Cheng, Y.F., 2021. A review on defect assessment of pipelines: principles, numerical solutions, and applications. Int. J. Pres. Ves. Pip. 191, 104329.

Qin, G., Huang, Y., Wang, Y., Cheng, Y.F., 2023. Pipeline condition assessment and finite element modeling of mechano-electrochemical interaction between corrosion defects with varied orientations on pipelines. Tunn. Undergr. Sp. Tech. 136, 105101.

Saadi, F.H., Lewis, N.S., McFarland, E.W., 2018. Correction: Relative costs of transporting electrical and chemical energy. Energy Environ. Sci. 11 (3), 714.

Shuai, Y., Zhang, X., Feng, C., Han, J., Cheng, Y.F., 2022. A novel model for prediction of burst capacity of corroded pipelines subjected to combined loads of bending moment and axial compression. Int. J. Pres. Ves. Pip. 196.

Sun, J., Cheng, Y.F., 2018. Assessment by finite element modeling of the interaction of multiple corrosion defects and the effect on failure pressure of corroded pipelines. Eng. Struct. 165, 278–286.

Sun, Y., Cheng, Y.F., 2022. Hydrogen-induced degradation of high-strength steel pipeline welds: a critical review. Eng. Fail. Anal. 133, 105985.

Sun, Y., Ren, Y., Cheng, Y.F., 2022. Dissociative adsorption of hydrogen and methane molecules at high-angle grain boundaries of pipeline steel studied by density functional theory modeling. Int. J. Hydrogen Energ. 47 (97), 41069–41086.

Titov, A.I., Lun-Fu, A.V., Bubenchikov, M.A., Gayvaronskiy, A.V., Bubenchikov, A.M., Lider, A.M., Syrtanov, M.S., Kudiiarov, V.N., 2019. Hydrogen accumulation and distribution in pipeline steel in intensified corrosion conditions. Materials 12 (9), 1409.

Wang, Y., Xia, A., Qin, G., 2022. Probabilistic modeling for reliability analysis of buried pipelines subjected to spatiotemporal earthquakes. Probabilist. Eng. Mech. 69, 103315.

Wang, H., 2018. Study on the Hydrogen Embrittlement Sensitivity of X100 Pipeline Steel. Tianjin University [Dissertation], Tianjin.

Wang, Y., Zhang, P., Hou, X., Qin, G., 2020. Failure probability assessment and prediction of corroded pipeline under earthquake by introducing in-line inspection data. Eng. Fail. Anal. 115, 104607.

Wijewickreme, D., Karimian, H., Honegger, D., 2009. Response of buried steel pipelines subjected to relative axial soil movement. Can. Geotech. J. 46 (7), 735–752.

Xu, L.Y., Cheng, Y.F., 2012. Reliability and failure pressure prediction of various grades of pipeline steel in the presence of corrosion defects and pre-strain. Int. J. Pres. Ves. Pip. 89, 75–84.

Zhang, H., Tian, Z., 2022. Failure analysis of corroded high-strength pipeline subject to hydrogen damage based on FEM and GA-BP neural network. Int. J. Hydrogen Energ. 47 (7), 4741–4758.

Zhang, S., Zhou, W., 2022. Assessment of the interaction of corrosion defects on steel pipelines under combined internal pressure and longitudinal compression using finite element analysis. Thin Wall. Struct. 171, 108771.